Calculation of the recoilless γ-ray emission spectra from a substitutional cation impurity diffusing via the ⟨001⟩ channels in the rutile structure

K. Ruebenbauer,* U. D. Wdowik, and M. Kwater
Institute of Physics and Computer Science, Pedagogical University, PL-30-084 Cracow, ul. Podchorążych 2, Poland
(Received 16 October 1995; revised manuscript received 11 March 1996)

The large anisotropy of the diffusion coefficient for a substitutional randomly diluted cationic impurity in the rutile structure, with the diffusivity being much larger along the tetragonal axis as compared to the diffusivity within a tetragonal plane, indicates that open and almost empty ⟨001⟩ channels are involved along with an interstitialcy mechanism to originate diffusion events leading an impurity from one to another substitutional cationic site. This model is used to evaluate the resulting emission Mössbauer spectra of the impurity staying locally at equilibrium with the lattice and embedded in a single-crystalline sample. Final results are shown for the 14.4 keV Mössbauer line in ^{57}Co (Fe). It is shown that channel diffusivity is governed by the exponential law, and details of the electric-field-gradient relaxation due to the diffusive motion of the probe are described from first principles. [S0163-1829(96)06430-2]

I. INTRODUCTION

Measurements of the diffusion coefficient tensor for highly diluted and randomly distributed substitutional cationic impurities in the rutile structure (an almost stoichiometric TiO_2-rutile is a well-known example) indicate for many such impurities a very large anisotropy, with the diffusivity being much larger along the tetragonal axis as compared to the diffusivity in the tetragonal plane.[1] Figure 1 shows details of the rutile structure, and one can easily identify open and almost empty channels along ⟨001⟩ direction. Since the anionic lattice is almost completely filled and the anions are immobile at the interesting time scale, one can conclude that a very small fraction of cations remains in the potential minima in the channels, creating a small fraction of randomly distributed substitutional cationic vacancies (some of them are due to the very diluted and randomly distributed impurities described above). Hence, an impurity could be forced into a channel via the interstitialcy mechanism after having ''encountered'' some cation in the channel (mainly cations constituting cationic lattice), perform some number of jumps within a channel, and finally jump into a substitutional site via another interstitialcy event. A cation forced into a channel via the last event goes away quite rapidly leaving the impurity in the unperturbed state (it is mainly a cation constituting lattice).

One can assume that for such a scenario the impurity remains locally at equilibrium with the lattice provided the temperature is high enough (the process is thermally driven anyway and the diffusivity has to be significant enough to be observable). Due to the fact that channels remain almost empty and the bulk of impurities are substitutional, the whole event described above takes a very short time compared to the average time period between successive such events. Events remain uncorrelated with each other as long as the lattice is not far from being perfect.

Hence, one can summarize the diffusivity model in the following way: a very diluted (isolated) impurity spends most of the time at the substitutional cationic site [called further (R), i.e., a regular site]. A very small fraction of the host cations happens to be in the almost empty channels moving rapidly along them. Corresponding cation vacancies are very sparse as the crystal is almost stoichiometric. Anions fill completely their sublattice and remain immobile. Sometimes a host cation moving along the channel gets in the vicinity of the impurity and subsequently kicks it into a channel filling its place (this is an intersticialcy mechanism, but one cannot exclude a small fraction of impurities jumping into the channel via the interstitial mechanism). Jumps of the impurity into almost empty channels occur with the average frequency ω_D. Each (R) site is surrounded by eight channel sites [called further (C) sites, i.e., channel sites] and hence, impurity jumps into a particular (C) site having an (R) impurity in the neighborhood occur with the frequency $\frac{1}{8}\omega_D$. Once the impurity has gotten into a channel it can jump along the channel (vertically) either up or down. These jumps occur with the average frequency ω_0. Hence, a frequency of jumps in the channel equals $2\omega_0$ as there are two possible such jumps—up or down. After many such in-the-channel jumps the impurity kicks some (R) cation (usually, a host cation) into one of the surrounding channels and fills its place. The host cation goes away along its channel. A frequency of the out-of-channel jumps is called ω_1. Due to the fact that each (C) site is surrounded by four (R) sites a jump into a particular (R) site occurs with the frequency $\frac{1}{4}\omega_1$.

The whole process described above constitutes a single diffusive event short compared to the average time period between such uncorrelated events occurring with the frequency ω_D. Hence, no measurable signal comes from (C) sites and all the signal comes exclusively from impurities residing on the (R) sites. A frequency $\omega_1 \gg \omega_D$ as otherwise a significant fraction of impurities would stay in the channel. Therefore there is no separate access to ω_1 and ω_0 frequencies and one can measure only a ratio defined here as $R=(2\omega_0)/\omega_1$. This ratio can take on any positive value in the model. Finally, one has to realize that the overall diffusivity is governed by the first step initiating the event, i.e., by a jump into the channel occurring with the frequency ω_D.

One can conclude this section by saying that potential

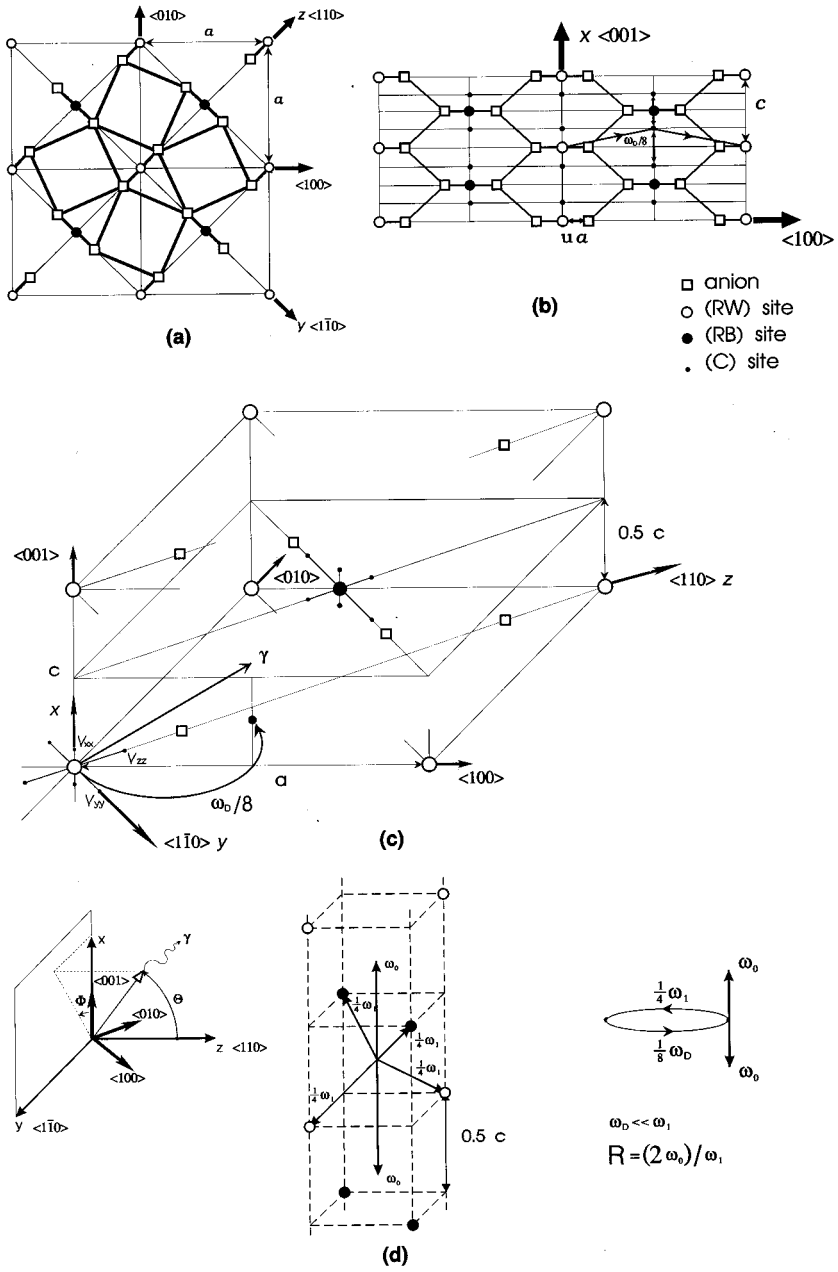

FIG. 1. Details of the rutile structure: (a) view ''down'' the tetragonal axis, (b) ''side'' view, (c) ''panoramic'' view of the chemical unit cell, (d) adopted polar and azimuthal angles shown in respect to the crystal axes, ''panoramic'' view of the ⟨001⟩ channel and diagram of the impurity jumps; u stands for the oxygen parameter, while the remaining symbols are explained within the text. Usually $u \cong 0.3$.

minima within channels form an almost empty simple tetragonal Bravais lattice (C), while the cations form a tetragonal body-centered Bravais lattice (R), the latter having two inequivalent sites (corners and centers, respectively) as far as the orientation of the local symmetric and even tensors of the second (or higher) order is considered [called further (RW)—white sites (corners) and (RB)—black sites (centers)]. However, the occupancy of both sites is equal to each other. All (R) cationic sites have local inversion centers. The scenario outlined above applies as well to the cases where the average distance traveled within a channel is quite disparate for impurities and host cations.

One has to note that each event has a 50% chance to change a color of the impurity. Hence, a color-switching frequency (relaxation frequency) equals $\frac{1}{2}\omega_D$. Positions in the channel do not depend upon the oxygen parameter (defined here as the ''Ti-O'' bond length projected on the edge of the chemical unit cell in the tetragonal plane and divided by the lattice constant in the tetragonal plane) and hence, the whole model depends upon the following parameters: ω_D, R, a, and c, where a stands for the lattice constant in the tetragonal plane (transversal constant) and c stands for the lattice constant along the tetragonal axis. Lattice constants can be removed by using scaled coordinates, while the frequency ω_D is no longer needed once the impurity has already jumped into the channel. Hence, a motion in the channel is completely described by the parameter R provided an impurity spends a short time in the channel as compared to the average residence time on the (R) site.

Experimental data of Sasaki, Peterson, and Hoshino[1] for iron in TiO_2-rutile indicate that $R \cong 100$ for that case and that the ratio R is practically temperature independent for this system. The paper is organized as follows: Section II deals with the details of the channel diffusivity mechanism, Sec. III is devoted to the calculation of the diffusion coefficient tensor, while Sec. IV describes a diffusion self-correlation

function of the impurity. Nonequivalence of the two sites is treated in Secs. V and VI, where the relaxation of the electric-field gradient and differences in the recoilless fraction (for a single crystal) are described, respectively. Section VII describes evaluation of the observable quantity, i.e., a Mössbauer spectrum obtainable from the impurities, while Sec. VIII summarizes the results.

II. DIFFUSIVITY IN A CHANNEL

Let us consider the following problem. An isolated impurity is forced (via the predominantly interstitialcy mechanism) into a straight, both ends infinite, and empty channel consisting of identical one-dimensional cells. Subsequently, an impurity can jump to the adjacent cells (with equal probabilities) or leave the channel (via a similar mechanism as mentioned above). An independent diffusive event[2] starts at the moment of the impurity jump into the channel and ends at the moment of the impurity jump out of channel. The situation can be illustrated as follows:

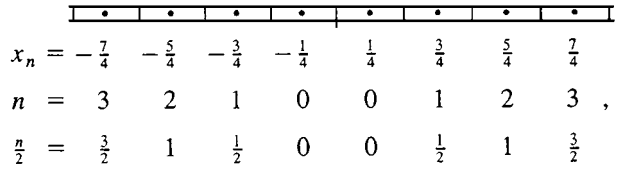

x_n	$-\frac{7}{4}$	$-\frac{5}{4}$	$-\frac{3}{4}$	$-\frac{1}{4}$	$\frac{1}{4}$	$\frac{3}{4}$	$\frac{5}{4}$	$\frac{7}{4}$
n	3	2	1	0	0	1	2	3
$\frac{n}{2}$	$\frac{3}{2}$	1	$\frac{1}{2}$	0	0	$\frac{1}{2}$	1	$\frac{3}{2}$

(1)

where the midpoint of the channel is taken at random. The coordinate x_n is defined in such a way to be consistent with the rutile structure $\langle 001 \rangle$ channels. There are three jump frequencies describing a problem. Namely, a jump frequency into any surrounding channel ω_D, a jump frequency within the channel ω_0, and the jump frequency out of channel ω_1. The first frequency stands here for the scaling frequency ω_D of the diffusive self-correlation function as it originates the whole sequence of jumps constituting a diffusive event (due to the fact that the channel remains practically empty there is no bunching effect).[2] The frequency $\omega_D \ll \omega_1$ due to the fact that the channel remains practically empty and the impurity spends most of the time at the substitutional (R) site. The remaining frequencies except ω_D cannot be measured separately in the event approximation[3] and hence, the following measurable ratio has to be defined (for details see, Fig. 1):

$$R = (2\omega_0)/\omega_1 . \tag{2}$$

Factor 2 is due to the fact that each cell is surrounded by two adjacent cells and the ratio R is positive for all physically meaningful situations. Hence, the problem can be described by a single (positive) parameter R except such trivial parameters like physical cell dimensions and scaling frequency ω_D. It has to be noted, that the arbitrary midpoint is a symmetry point of the channel.

Hence, one has to find an impurity distribution along the channel—being symmetrical with respect to the midpoint and depending upon the single parameter R. A probability to jump to the adjacent cell can be expressed as follows:

$$p = R/[2(1+R)], \tag{3}$$

while the probability to leave the channel from a given cell equals $1-2p$. Each impurity jump within a channel creates a new generation m dependent only upon a previous generation. The index $m=0, 1, 2, \ldots$ enumerates subsequent generations, where $m=0$ generation is the oldest generation occurring just after the impurity jump into the channel. Hence, the weight at coordinate x_n for the $m+1$ generation can be calculated as follows:

$$W_{m+1}(x_n) = p\left[W_m\left(x_n - \frac{1}{2} \right) + W_m\left(x_n + \frac{1}{2} \right) \right],$$

where

$$W_0\left(x_n = +\frac{1}{4} \right) = W_0\left(x_n = -\frac{1}{4} \right) = \frac{1}{2}$$

and

$$W_0\left(x_n \neq +\frac{1}{4}, -\frac{1}{4} \right) \equiv 0 \tag{4}$$

due to the midpoint symmetry. It has to be noted, that

$$W_m(x_n) = W_m(-x_n) \quad \text{and} \quad W_m(x_n) \geqslant 0. \tag{5}$$

Hence, one can calculate new weights in terms of the index n in the following way:

$$W_{mn} = W_m(x_n) + W_m(-x_n), \tag{6}$$

where $x_n = (1+2n)/4$. One has to note that the weight of the generation m equals $(2p)^m$ and it can be calculated as follows:

$$\sum_{n=0}^{\infty} W_{mn} = (2p)^m. \tag{7}$$

Hence, a normalized distribution within a channel can be obtained by summation over all generations and taking a proper normalization, i.e.,

$$\rho_n = (1-2p) \sum_{m=0}^{\infty} W_{mn}, \tag{8}$$

where $\rho_n \geqslant 0$ and $\Sigma_{n=0}^{\infty} \rho_n = 1$. Expressions (4) and (6) allow us to calculate weights W_{mn} in the following way:

$$W_{mn} = p^m C_{mn}, \tag{9}$$

where $C_{mn} \equiv 0$ for $n > m$ and otherwise C_{mn} are expressible in terms of the Newtonian symbols in the following way:

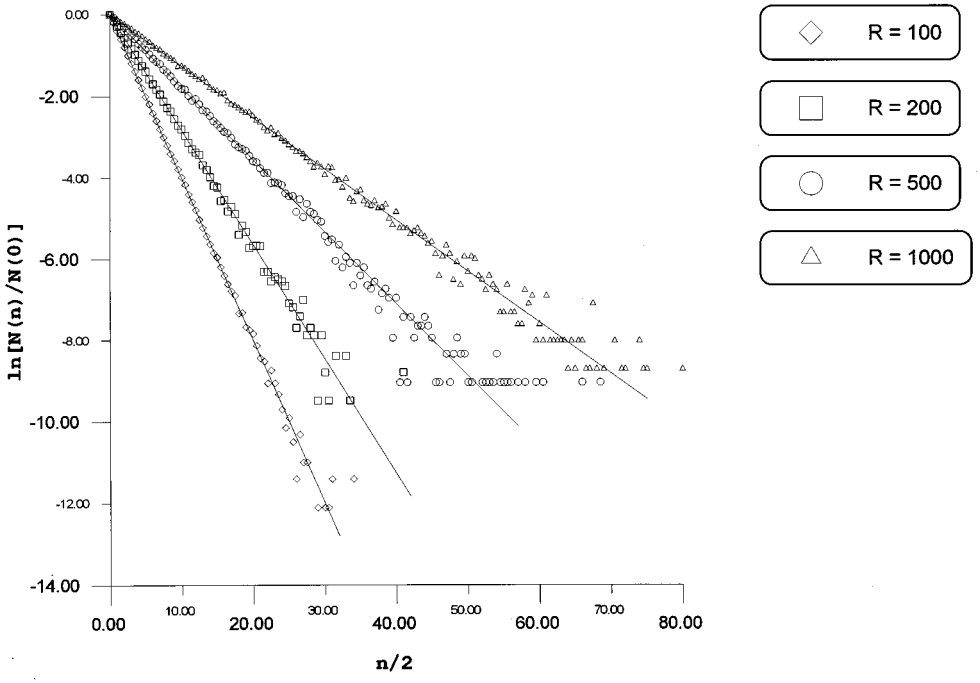

FIG. 2. Plot of the impurity distribution along the channel for several values of the parameter R. Distributions have been generated by the Monte Carlo method.

$m-$odd

$$n= \quad 0 \quad 1 \quad 2 \quad 3 \quad \ldots \quad m-1 \quad m$$

$$C_{mn}= \left[\binom{m}{\frac{m-1}{2}}, \binom{m}{\frac{m-1}{2}}, \left[\binom{m}{\frac{m-1}{2}-1}, \binom{m}{\frac{m-1}{2}-1}\right], \ldots, \left[\binom{m}{0}, \binom{m}{0}\right]\right]$$

$m-$even

$$n= \quad 0 \quad 1 \quad 2 \quad \ldots \quad m-1 \quad m$$

$$C_{mn}= \binom{m}{\frac{m}{2}}, \left[\binom{m}{\frac{m}{2}-1}, \binom{m}{\frac{m}{2}-1}\right], \ldots, \left[\binom{m}{0}, \binom{m}{0}\right], \tag{10}$$

$$\binom{m}{k}=\frac{m!}{k!(m-k)!}.$$

Several low-order C_{mn} coefficients are listed below:

$n=$	0	1	2	3	4
$m=0$	1	0	0	0	0
1	1	1	0	0	0
2	2	1	1	0	0
3	3	3	1	1	1
4	6	4	4	1	1
	. . . . .				

It is interesting to note that the following ratio is constant for the above-mentioned distribution:

$$\left(\sum_{m=0}^{\infty} p^m C_{m,n+1}\right) \Big/ \left(\sum_{m=0}^{\infty} p^m C_{mn}\right)=\mathbf{C}(R), \tag{11}$$

i.e., it does not depend upon the index n. Hence, the distribution (8) can be expressed as an exponential distribution of the following form:

$$\rho_n(\sigma)=\exp\{-[n/(2\sigma)]\} \Big/ \left(\sum_{n'=0}^{\infty} \exp\{-[n'/(2\sigma)]\}\right), \tag{12}$$

where $\sigma=\sigma(R)$ depends solely upon R and it is responsible for the ''width'' of the distribution.

We were unable to find any simple analytical expression for the function $\sigma(R)$. It probably does not exist at all as the channel space is quantized and it has properties of the fractal spaces as well. Hence, we have used a Monte Carlo method in order to generate the above-mentioned distribution. Figure 2 shows several distributions generated in such a way for different values of R. Here $N(n)$ stands for the number of

events, where the impurity left the channel at n. There is no doubt that the generated distributions are exponential. Figure 3 shows $\sigma(R)$ extracted from the above exponential distributions and plotted versus R. The latter function can be well approximated by fitting to the following phenomenological function:

$$\sigma(R)=\exp([1-\eta(x-x_0)]\{a_1+b_1x+C\ \exp[\alpha(x-x_0)]\}+\eta(x-x_0)\{a_2+b_2x+c_2\exp[\beta(x_0-x)]\}),$$
$$C=(a_2-a_1)+x_0(b_2-b_1)+c_2,\quad x=\ln(R),\quad x_0=\ln(R_0),\quad R\geqslant 0,\quad \sigma(R=0)=0,$$
$$a_1<0,\quad a_2<0,\quad x_0<0,\quad b_1>0,\quad b_2>0,\quad c_2>0,\quad \alpha>0,\quad \beta>0. \tag{13}$$

Here, $\eta(x-x_0)$ stands for the Heaviside function. The following values of the parameters fit optimally to the data:

$$x_0=-0.273,\quad R_0=\exp(x_0)=0.7611;$$

a_1	a_2	b_1	b_2	c_2	α	β
−2.46(4)	−1.403(4)	0.074(3)	0.5030(8)	0.174(4)	0.289(7)	0.74(3)

(14)

allowing us to obtain a very fast algorithm to calculate distribution (12) in terms of the parameter R.

The function $\sigma(R)$ approaches zero for R tending to zero and it increases with the increasing R. A ''flattening'' at small values of R is due to the quantum character of the channel space, i.e., due to the fact that the impurity cannot jump ''halfway'' between cells. This ''flattening'' is seen on the logarithmic scale used for abscissa and the function plotted. It has to be noted, that the above outlined formalism applies to infinite, both ends open channels having constant curvature as well.

III. DIFFUSION COEFFICIENT

In order to calculate a diffusion coefficient (straight channels) additional information about the channel surrounding is necessary. We confine ourselves to the ⟨001⟩ channels in the rutile structure and isolated impurities (diluted ones) diffusing via the channel mechanism between cation (R) sites. It is assumed that impurities and to some extent host cations are long-range mobile, while anions remain confined to the proper lattice sites. For such a case a diffusion coefficient is axially symmetric with both equivalent principal axes being perpendicular to the ⟨001⟩ direction. Hence, it is described by two components taking on the following forms:

$$D\langle 100\rangle=(1/8)\omega_D a^2$$

in the transverse direction and

$$D\langle 001\rangle=(1/16)\omega_D c^2\left(\sum_{n=0}^{\infty}\{\rho_n(\sigma)[2n(n+1)+1]\}\right)$$

in the vertical direction. An average diffusion coefficient equals

$$\langle D\rangle=\frac{1}{3}\{D\langle 001\rangle+2D\langle 100\rangle\}. \tag{15}$$

Here, $a>0$ stands for the chemical cell lattice constant in the transverse direction, while $c>0$ is the chemical cell lattice constant in the vertical direction. Directions ⟨100⟩, ⟨010⟩, and ⟨001⟩ define an orthogonal system as the chemical unit cell is tetragonal. The scaling frequency $\omega_D>0$. Hence, the anisotropy of the diffusion coefficient defined as $\delta=D\langle 001\rangle/D\langle 100\rangle$ depends only upon c/a and R and equals (see, Fig. 4)

$$\delta=\frac{1}{2}(c/a)^2\left(\sum_{n=0}^{\infty}\{\rho_n(\sigma)[2n(n+1)+1]\}\right)$$
$$\cong\frac{1}{2}(c/a)^2[1+1.00778R]. \tag{16}$$

The last approximation is accurate within about 0.9% for $R\leqslant 10^3$. It is convenient to define the following orthogonal right-handed reference frame: x along the ⟨001⟩, y along the ⟨110⟩, and z along the ⟨110⟩ direction in the case of rutile structure. A diffusion coefficient in the arbitrary direction can be expressed as follows in the above-mentioned reference frame:

$$D(\theta\phi)=D\langle 001\rangle\sin^2\theta\ \cos^2\phi$$
$$+D\langle 100\rangle(\sin^2\theta\sin^2\phi+\cos^2\theta), \tag{17}$$

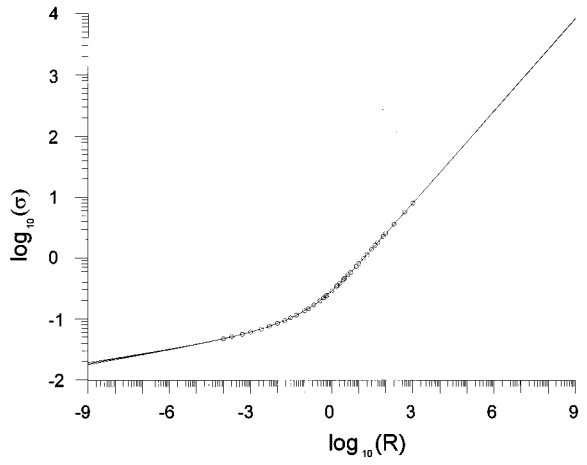

FIG. 3. Plot of the function $\sigma(R)$ fitted to the function described by expressions (13) and (14). Central line shows the most probable curve, while the upper and lower lines show uncertainties due to the finite statistics of the Monte Carlo simulations.

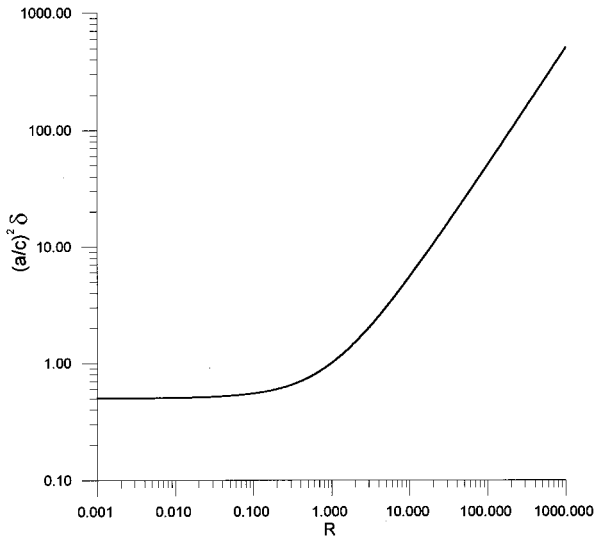

FIG. 4. Plot of the reduced anisotropy of the diffusion coefficient $(a/c)^2\delta$ versus parameter R (accordingly to the ''exact'' formula).

where $0\leqslant\theta\leqslant\pi$ stands for the polar angle and $0\leqslant\phi<2\pi$ stands for the azimuthal angle (see, Fig. 1).

In principle, the parameter R is temperature dependent. However, if the absolute value of the difference of the potential barriers for $\frac{1}{4}\omega_1$ and ω_0 jumps is much smaller than the barrier for the $\frac{1}{8}\omega_D$ jumps, it is likely that the former process is already saturated at temperatures high enough to observe any diffusivity. Hence, the parameter R becomes constant versus temperature and subsequently the anisotropy of the diffusion coefficient does not depend upon temperature as it is independent of the frequency ω_D, the latter being the only parameter strongly dependent upon temperature. Exactly such a behavior was observed by Sasaki, Peterson, and Hoshino[1] for iron in TiO_2-rutile, where the anisotropy of the diffusion coefficient corresponds to $R\cong100$ at all accessible temperatures, while the overall diffusivity follows the Arrhenius pattern. These results strongly favor the model outlined above.

IV. SELF-CORRELATION FUNCTION FOR DIFFUSION

The cation (R) sublattice is a single tetragonal body-centered Bravais lattice in the case of the rutile structure. Hence, a purely diffusional self-correlation function of the impurity is a scalar function and takes on the following form in the above mentioned reference frame:[4–12]

$$G(\overline{q},t)=\int_{-\infty}^{\infty}d^3re^{i\overline{q}\cdot\overline{r}}G(\overline{r},t)=\exp\{-\omega_D[1-\alpha(\overline{q})]t\}, \tag{18}$$

where $\overline{q}$ stands for the wave-vector transfer to the lattice, $t\geqslant0$ stands for time, and $G(\overline{r},t)$ denotes a probability density to find the impurity in the vicinity of the point $\overline{r}$ at time t provided it was in the origin at $t=0$. A geometrical factor $\alpha(\overline{q})$ is a Fourier transform of the spatial distribution of the impurity produced by the diffusive event, i.e.,

$$\alpha(\overline{q})=\int_{-\infty}^{\infty}d^3re^{i\overline{q}\cdot\overline{r}}\rho(\overline{r}),$$

where $\rho(\overline{r})$ stands for the probability density to find an impurity in the position $\overline{r}$ after the diffusive event provided it was in the origin before the event. A geometrical factor $\alpha(\overline{q})$ takes on the following form in the present model:

$$\alpha(\overline{q})=\sum_{n=0}^{\infty}\rho_n(\sigma)\{\mathbf{A}_1\cos[cq_xf_0(n)]+\mathbf{A}_2\cos[cq_xf_1(n)]\},$$

$$\mathbf{A}_1=(1/10)\{1+4\cos[(aq_y)/\sqrt{2}]\cos[(aq_z)/\sqrt{2}]\},$$

$$\mathbf{A}_2=(1/4)\{\cos[(aq_y)/\sqrt{2}]+\cos[(aq_z)/\sqrt{2}]\}, \tag{19}$$

$$f_0(n)=\frac{1}{2}(n+1)\quad\text{and}\quad f_1(n)=\frac{1}{2}n\quad\text{for } n \text{ odd},$$

and

$$f_0(n)=\frac{1}{2}n\quad\text{and}\quad f_1(n)=\frac{1}{2}(n+1)\quad\text{for } n \text{ even},$$

q_x,q_y,q_z are components of the wave-vector transfer to the lattice. For the emission Mössbauer spectroscopy components of the wave-vector transfer take on the form:

$$q_x=-q_0\sin\theta\cos\phi,$$

$$q_y=-q_0\sin\theta\sin\phi, \tag{20}$$

$$q_z=-q_0\cos\theta,$$

where $q_0>0$ stands for the wave number of the emitted γ-ray photon and θ, ϕ are polar and azimuthal angles of the emission direction, respectively [for the present case, the sign in expressions (20) could be dropped due to the presence of inversion centers]. Figure 5 shows $\gamma(\overline{q})=1-\alpha(\overline{q})$ plotted along arcs of great circles of the Ewald sphere for a constant wave number and lattice constants, and for different values of the parameter R. The function $\gamma(\overline{q})$ represents variability of the spectral width versus direction on the Ewald sphere. It can take on values from the range [0,2] and it approaches zero for the wave-vector transfer being equal to one of the reciprocal-lattice vectors. It is appropriate to call it a diagonal geometrical factor.

V. RELAXATION OF THE ELECTRIC-FIELD GRADIENT

For an isolated unperturbing impurity located at the (R) site in the rutile structure and otherwise almost perfect cation lattice, perfect anion lattice, and negligible concentration of interstitials, all impurity sites are equivalent as far as scalar hyperfine interactions are considered (including second-order Doppler shift). However, nonscalar electric hyperfine interactions (magnetic interactions are absent) break symmetry generating two (RW) and (RB) simple tetragonal sublattices[12] having an equal number of otherwise equivalent kernels. Both of these two sublattices are equally populated by the impurities. A semiclassical electric quadrupole interaction is the only one being able to split sufficiently nuclear levels and the electric-field gradient (EFG) tensor has no axial symmetry on the (R) sites.[13] On the other hand, prin-

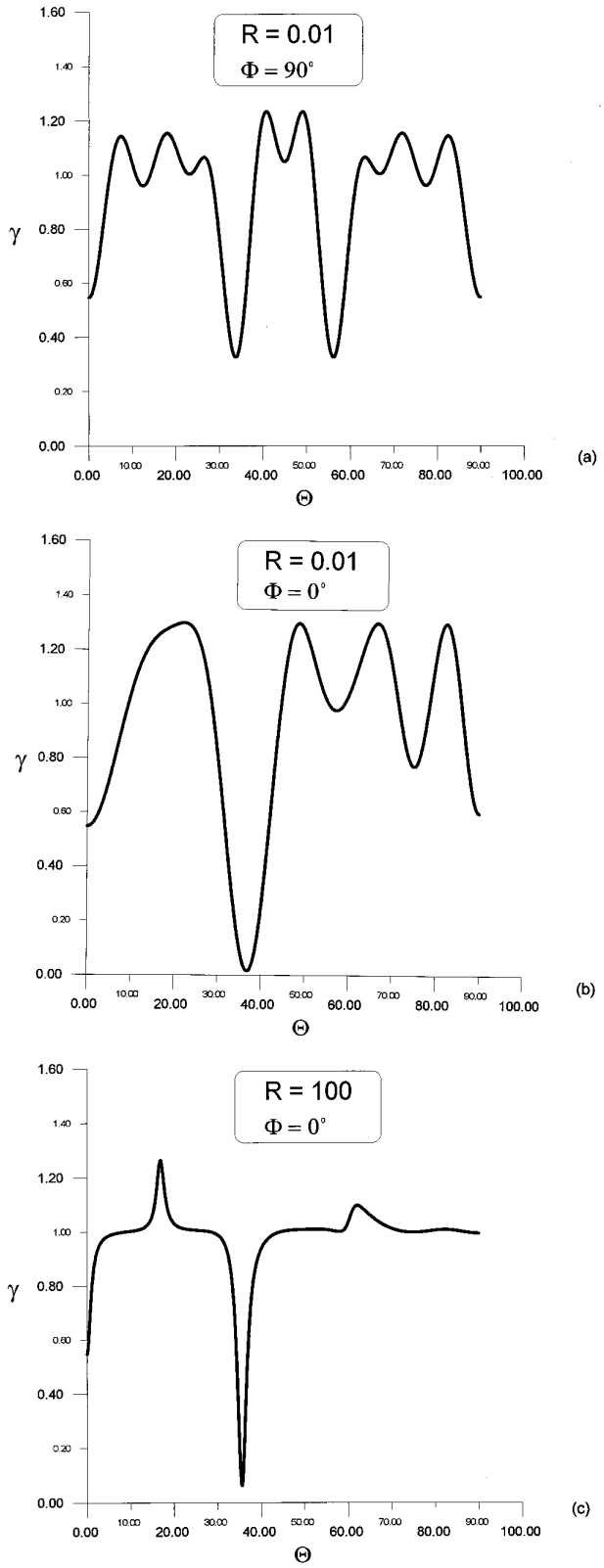

FIG. 5. $\gamma(\overline{q})$ plotted along various arcs of great circles of the Ewald sphere for $a=4.594$ Å, $c=2.959$ Å, and $q_0=7.30254$ Å^{-1}: (a) from $\langle 110\rangle$ to $\langle \bar{1}10\rangle$ direction, (b) from $\langle 110\rangle$ to $\langle 001\rangle$ direction at small R, (c) from $\langle 110\rangle$ to $\langle 001\rangle$ direction at large R; it has to be noted, that curve (a) does not depend upon the particular value of R, while curve (c) clearly shows an ''interference'' pattern due to the very long distance traveled within a channel.

cipal axes of the EFG tensor coincide with the axes of the previously defined reference frame for both (RW) and (RB) sites. Namely, the EFG (traceless) tensor takes on the following form in the above-mentioned reference frame (see, Fig. 1):

$$\hat{V}_1=\begin{pmatrix} V_{xx} & 0 & 0 \\ 0 & -(V_{xx}+V_{zz}) & 0 \\ 0 & 0 & V_{zz} \end{pmatrix} \quad \text{for } (RW) \text{ site ''1''}$$

and

$$\hat{V}_2=\begin{pmatrix} V_{xx} & 0 & 0 \\ 0 & V_{zz} & 0 \\ 0 & 0 & -(V_{xx}+V_{zz}) \end{pmatrix} \quad \text{for } (RB) \text{ site ''2''}, \tag{21}$$

where V_{xx} and V_{zz} stand for the EFG along the x and z axes, respectively, and $V_{yy}=-(V_{xx}+V_{zz})$. Components of the EFG are defined here for the (RW) site. It is interesting to note that these two tensors transform one into another by a right angle rotation around the $\langle 001\rangle$ axis. Hence, in the ''static'' limit they produce the same set of eigenvalues. On the other hand, in the extremely fast relaxation limit they average to the axially symmetric EFG tensor having an axial symmetry in the plane perpendicular to the $\langle 001\rangle$ axis, i.e.,

$$\langle \hat{V}\rangle=\frac{1}{2}(\hat{V}_1+\hat{V}_2)=V_{xx}\begin{pmatrix} 1 & 0 & 0 \\ 0 & -\frac{1}{2} & 0 \\ 0 & 0 & -\frac{1}{2} \end{pmatrix}. \tag{22}$$

Relaxation between these two sites occurs solely due to the diffusive events and 50% of events lead to the sites of the opposite ''color.'' Hence, the diffusion/relaxation matrix is Hermitian and has the following form:[11,12]

$$\hat{R}(\overline{q})=\omega_D\begin{pmatrix} -\left[\gamma(\overline{q})+\frac{1}{2}\right] & \frac{1}{2} \\ \frac{1}{2} & -\left[\gamma(\overline{q})+\frac{1}{2}\right] \end{pmatrix} \tag{23}$$

as the energy of the electric quadrupole interaction is much smaller than the energy of the diffusive motion. Thus, the quadrupolar relaxation frequency equals $(1/2)\omega_D$. It is interesting to note that even for the wave-vector transfer being equal to one of the reciprocal-lattice vectors G, the Mössbauer spectrum is still sensitive to the diffusive motion via the quadrupolar relaxation mechanism. For the latter case the operator $\hat{R}(\overline{q})$ takes on the following form:[12,14,15]

$$\hat{R}(\overline{q}=\overline{G})=\frac{1}{2}\omega_D\begin{pmatrix} -1 & 1 \\ 1 & -1 \end{pmatrix}. \tag{24}$$

VI. RECOILLESS FRACTION

All unperturbed (R) cation sites have inversion centers and hence, only even vibrational tensors do not vanish.[16,17] For relatively small wave-number transfers a contribution from higher terms than quadratic seems to be negligible.[18] It is reasonable to assume as well, that the vibrational dynamics is non-Gaussian only during the encounter with the inter-

stitial atom. The latter event is short compared to the average time between such events. Both (RW) and (RB) sites have the same average recoilless fraction and hence, the anisotropy of the recoilless fraction is solely responsible for the modification of the relative line intensities, particularly due to the fact that (RW) and (RB) sites are equally populated (the line splitting is caused here by the EFG). Quadratic tensors describing recoilless fraction are diagonal for both sites in the reference frame used above. They have the following forms:[17]

$$\hat{B}_1=\begin{pmatrix} B_{xx} & 0 & 0 \\ 0 & B_{yy} & 0 \\ 0 & 0 & B_{zz} \end{pmatrix} \quad \text{for } (RW) \text{ site ``1''}$$

and

$$\hat{B}_2=\begin{pmatrix} B_{xx} & 0 & 0 \\ 0 & B_{zz} & 0 \\ 0 & 0 & B_{yy} \end{pmatrix} \quad \text{for } (RB) \text{ site ``2''}, \tag{25}$$

where B_{xx}, B_{yy}, and B_{zz} stand for the mean-squared displacements along the x, y, and z axes, respectively. Components of the vibrational tensor are defined here for the (RW) site. Hence, the recoilless fraction in the direction of the emitted photon can be expressed as follows for (RW) and (RB) sites, respectively:

$$\begin{aligned} f_1(\overline{q})=f_1(\theta\phi)=\exp\{-q_0^2[&B_{xx}\sin^2\theta\cos^2\phi \\ &+B_{yy}\sin^2\theta\sin^2\phi+B_{zz}\cos^2\theta]\}, \\ f_2(\overline{q})=f_2(\theta\phi)=\exp\{-q_0^2[&B_{xx}\sin^2\theta\cos^2\phi \\ &+B_{zz}\sin^2\theta\sin^2\phi+B_{yy}\cos^2\theta]\}, \end{aligned} \tag{26}$$

where q_0, θ, and ϕ are defined by expression (20).

A diffusive motion tends to mix colors of the impurities and hence, diagonal terms expressed by Eqs. (26) have to be supplemented by the off-diagonal (mixing) terms. Due to the fact that the characteristic time scale of the vibrational dynamics is much shorter than the time scale of the diffusive motion, an independent dynamics approximation can be used.[12,19] Hence, the off-diagonal terms are simply expressed by the geometrical averages of the respective diagonal terms and the weighting operator takes on the following (symmetric) form:

$$\hat{f}(\theta\phi)=\begin{pmatrix} f_1(\theta\phi) & [f_1(\theta\phi)f_2(\theta\phi)]^{1/2} \\ [f_2(\theta\phi)f_1(\theta\phi)]^{1/2} & f_2(\theta\phi) \end{pmatrix}. \tag{27}$$

The weighting operator (27) cannot be uniquely determined from a single spectrum obtained at the well-defined wave-vector transfer. Hence, it has to be transformed to the following form:

$$\hat{f}(\theta\phi)=f_1(\theta\phi)\begin{pmatrix} 1 & [f_2(\theta\phi)/f_1(\theta\phi)]^{1/2} \\ [f_2(\theta\phi)/f_1(\theta\phi)]^{1/2} & [f_2(\theta\phi)/f_1(\theta\phi)] \end{pmatrix},$$

where

$$f_2(\theta\phi)/f_1(\theta\phi)=\exp\{q_0^2\Delta_0[1-\sin^2\theta(1+\sin^2\phi)]\}$$

with

$$\Delta_0=B_{zz}-B_{yy}. \tag{28}$$

The anisotropy parameter Δ_0 can be determined from the shape of a single spectrum provided the spectrum is observed far away from the great circle of the Ewald sphere passing through the $\langle 001\rangle$ direction and either the $\langle 100\rangle$ or $\langle 010\rangle$ directions.

VII. SPECTRUM CALCULATION

Calculation of the Mössbauer spectrum shape for an emission spectroscopy from a single crystal in a standard transmission geometry can be performed in a rather straightforward manner provided the following conditions are satisfied:

(1) resonance absorption within source is negligible;[20]

(2) direction of the emitted γ-ray beam is well defined;

(3) an unbroadened, single line, flat and homogeneous, unpolarizing absorber is used;

(4) absorber is resonantly thin and vibrates along the γ-ray beam with a small amplitude and frequency low enough to avoid phase modulation;

(5) intensity of radiation reemitted from the absorber and reaching the detector is negligible;

(6) detector and counting electronics stay within a linear-response range;

(7) an emitting atom stays at equilibrium with the lattice and temperature is high enough to equalize the population of the hyperfine levels, e.g., all after effects should vanish at a time scale short compared to the time scale of the Mössbauer transition.

The first task is to calculate the superoperator (Liouville operator) of the problem and hence, one has to start from the super-Hamiltonian. A hyperfine Hamiltonian can be expressed as follows:[21]

$$\hat{H}=\left(\frac{\mathbf{e}Q}{4I(2I-1)}\right)\sum_{ij=1}^{3} V_{ij}\left(\hat{I}_i\hat{I}_j+\hat{I}_j\hat{I}_i-\frac{2}{3}\,\delta_{ij}\hat{I}^2\right) \tag{29}$$

for an electric quadrupole interaction, where $\mathbf{e}$ denotes an elementary positive charge, Q stands for the intrinsic spectroscopic nuclear electric quadrupole moment (pointlike approximation), I denotes nuclear spin (for $I\leqslant 1/2$ the Hamiltonian is a zero matrix), indices i,j enumerate coordinate axes of the above mentioned reference frame in the order xyz, while symbols $\hat{I}_i$ and $\hat{I}_j$ stand for the appropriate spin-projection operators, and $\hat{I}^2$ denotes a total spin operator

squared. V_{ij} stand for the appropriate components of the symmetric (traceless) electric-field-gradient tensor. One has to note that four such Hamiltonians appear in the present problem, i.e., for the ground and excited nuclear states and for the (*RW*) and (*RB*) sites as well. Hence, one has to deal with two quadrupole moments and two spins. A super-Hamiltonian takes on the form[12,14]

$$H_s^x(m_e m_g m_e' m_g') = \delta(m_e m_e') H_g^{(s)}(m_g m_g') - \delta(m_g m_g') \times [H_e^{(s)}(m_e m_e') + \delta(m_e m_e') S], \quad (30)$$

where the index s refers to the site ($s=1,2$), indices e,g refer to the excited and ground state; respectively, m_e and m_g stand for the respective magnetic quantum numbers, and S denotes a total spectrum shift with respect to the absorber used. The matrix element of the superoperator $\hat{\mathbf{R}}$ can be expressed as follows:[12,14]

$$R(ss' m_e m_g m_e' m_g') = \delta(m_e m_e')\delta(m_g m_g') R_{ss'}(\overline{q}) + i\delta(ss') H_s^x(m_e m_g m_e' m_g'), \quad (31)$$

where $R_{ss'}(\overline{q})$ stands for the matrix element of the operator, Eq. (23). It has to be noted that this superoperator is a linear combination of the Hermitian matrices (weights of all-involved states are equal each to other). However, eigenvalues are complex numbers. The superoperator has the dimensions

$$\nu_0 \otimes \nu_0 = [2(2I_e+1)(2I_g+1)] \otimes [2(2I_e+1)(2I_g+1)]$$

with

$$\nu_0 = 2(2I_e+1)(2I_g+1)$$

as there are two relaxation states, $2I_e+1$ excited hyperfine levels and $2I_g+1$ ground hyperfine levels. The superoperator describes all the physics involved except vibrational dynamics and the initial population of the eigenstates, the latter being equal to each other in the present case.

Line intensities of the recoilless γ-ray resonant radiation emitted from the source can be expressed in the following way:[22]

$$C_\nu(\overline{q}) = \sum_{k=\pm 1} \sum_{m_e m_e'} \sum_{m_g m_g'} \sum_{LL'} \delta_L \delta_{L'} \times \langle L' m_g' | \hat{T}_{pk}(\theta\phi) | m_e' \rangle^* \langle L m_g | \hat{T}_{pk}(\theta\phi) | m_e \rangle \times \sum_{ss'} f_{ss'}(\theta\phi) v_{\nu s' m_e' m_g'}(\overline{q}) u_{\nu s m_e m_g}(\overline{q}), \quad (32)$$

where the index $\nu=1,2,\ldots,\nu_0$ enumerates eigenstates of the problem, L denotes an angular momentum transfer during the nuclear decay, $\delta_L=1$ for dipolar or quadrupolar transitions, while for the mixed transitions (dipolar/quadrupolar) $\delta_1=1$ and δ_2 stands for the intrinsic nuclear mixing ratio for the single photon radiative decay to the ground state (real number), k enumerates polarization states of the radiation (due to the fact that an unpolarizing single line absorber is used, off-diagonal terms vanish), symbols $\hat{T}_{pk}(\theta\phi)$ represent multipole operators of the parity p ($p=0$ for even transitions and $p=1$ for odd transitions), polarization k, and in the direction $\theta\phi$ defined in the above-mentioned reference frame. Finally, $v_{\nu s' m_e' m_g'}(\overline{q})$ and $u_{\nu s m_e m_g}(\overline{q})$ represent left and right eigenvector coefficients of the superoperator, respectively, while $f_{ss'}(\theta\phi)$ is a matrix element of the weighting operator (27) or (28). Matrix elements of the multipole operators satisfy the following relationship:[17,22]

$$\langle L m_g | \hat{T}_{pk}(\theta\phi) | m_e \rangle = \chi(Lkp) C(I_g L - m_g M | I_e m_e) \times d_{kM}^L(\theta) e^{iM\phi};$$

where

$$\chi(Lkp) = [(2L+1)/2]^{1/2} (-1)^{\delta(-1,k)\delta[-1,(-1)^{p+L-1}]} \times i^{\delta[-1,(-1)^{p+L-1}]}, \quad (33)$$

$M=m_e-m_g$, $d_{kM}^L(\theta)$ denotes a spherical operator matrix element and $C(I_g L - m_g M | I_e m_e)$ represents a Clebsch-Gordan coefficient. In order to calculate a spectrum shape it is practical to renormalize line intensities and to calculate linewidths in the following way:[22]

$$b_\nu(\overline{q}) = C_\nu(\overline{q}) \Big/ \sum_{\nu'=1}^{\nu_0} \mathrm{Re}[C_{\nu'}(\overline{q})]$$

and

$$\Gamma_\nu(\overline{q}) = \Gamma - 2\,\mathrm{Re}[\lambda_\nu(\overline{q})], \quad (34)$$

where Γ denotes a total (source) linewidth in the ''static'' limit ($\omega_D=0$), while $\lambda_\nu(\overline{q})$ stands for the νth eigenvalue of the superoperator. The spectrum shape can be calculated now in a straightforward manner. Namely, it takes on the following form:[23,24]

$$P(\overline{q}v) = B_0 \left[1 - f_S(\overline{q}) + f_S(\overline{q}) \left(\int_{-\infty}^{\infty} d\omega \rho(\overline{q}\omega, v) e^{-t\mathscr{L}(\omega)} \right) \right]$$

with

$$\mathscr{L}(\omega) = \{1 - [(2\xi)/\Gamma_0]\omega\} / \{1 + [(2/\Gamma_0)\omega]^2\}, \quad (35)$$

and a recoilless radiation density being expressed as

$$\rho(\overline{q}\omega, v) = (2\pi)^{-1} \sum_{\nu=1}^{\nu_0} \left(\frac{\Gamma_\nu(\overline{q})\mathrm{Re}[b_\nu(\overline{q})] + 2\alpha_\nu(\overline{q})\mathrm{Im}[b_\nu(\overline{q})]}{[(1/2)\Gamma_\nu(\overline{q})]^2 + [\alpha_\nu(\overline{q})]^2} \right),$$

where

$$\alpha_\nu(\overline{q}) = \omega + v + \mathrm{Im}[\lambda_\nu(\overline{q})].$$

Here v stands for the Doppler velocity (energy) applied by the spectrometer, B_0 denotes the number of counts far off resonance—in a standard multiscaler setup, t stands for the effective resonant absorber thickness (dimensionless—eventually corrected for the intrinsic absorber broadening), ξ stands for an effective interference term due to the absorber[17,22,25–27] and Γ_0 is the absorber linewidth (natural). An effective recoilless fraction of the source $f_S(\overline{q})$ is a weighted average over all sites, with a common wave-vector transfer to the system $\overline{q}$, corrected for the detector background under the Mössbauer γ-ray line. Hence, it takes on the following form for the rutile structure:

$$f_S(\overline{q}) = \frac{1}{2}\lambda^{-1}[f_1(\overline{q}) + f_2(\overline{q})], \tag{36}$$

where $f_1(\overline{q})$ and $f_2(\overline{q})$ stand for recoilless fractions of the respective sites, see, expression (26), and $\lambda = (s_0 + b_0)/s_0$ with s_0 being a detector signal due to the Mössbauer γ-ray line (both quasielastic and inelastic components) and b_0 being a total detector background under the selected Mössbauer γ-ray line.[17] A recoilless radiation density $\rho(\overline{q}\omega, v)$ takes on non-negative value for any value of the arguments (and for any polarization as well) and it is normalized to unity, i.e.,

$$\int_{-\infty}^{\infty} d\omega \rho(\overline{q}\omega, v) \equiv 1.$$

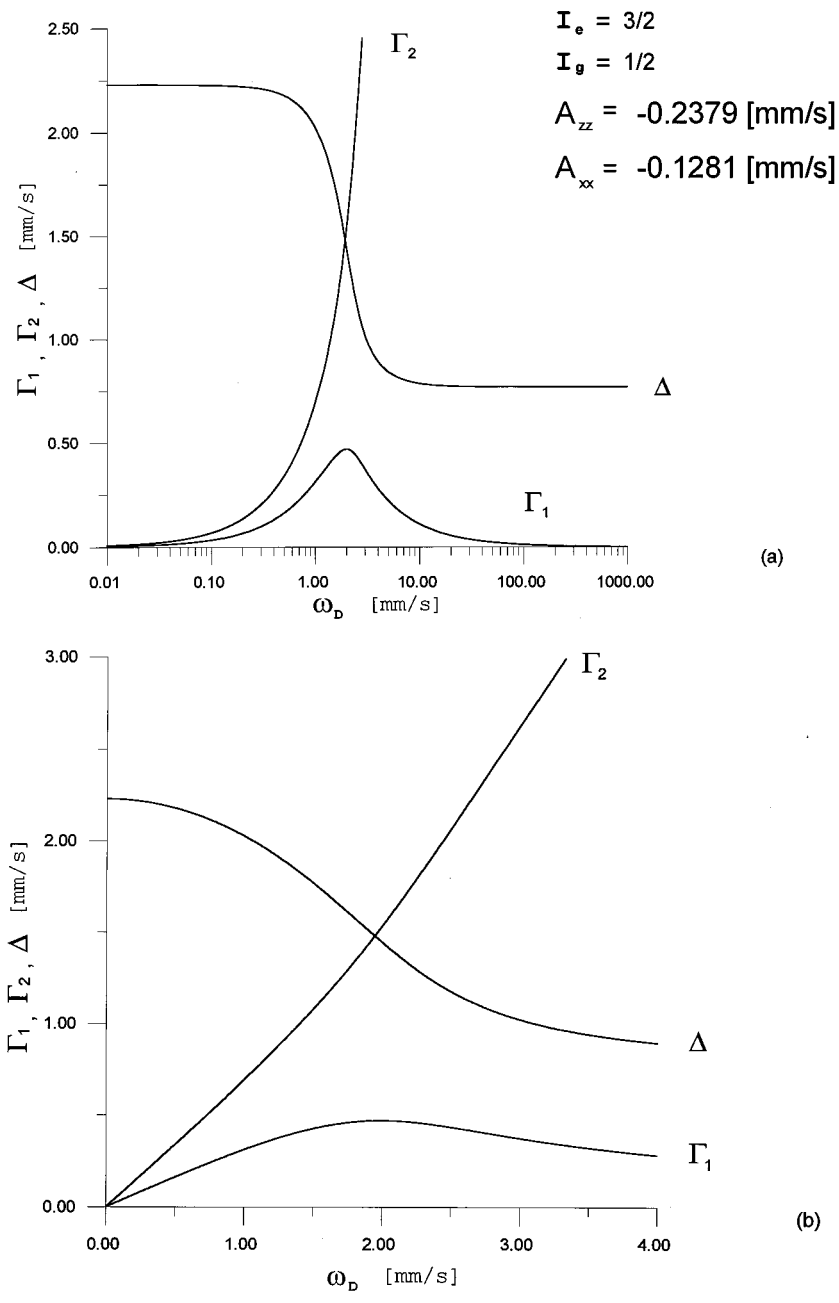

FIG. 6. Γ_1, Γ_2, and Δ (splitting) plotted versus ω_D: (a) broad range of ω_D, (b) narrow range of ω_D.

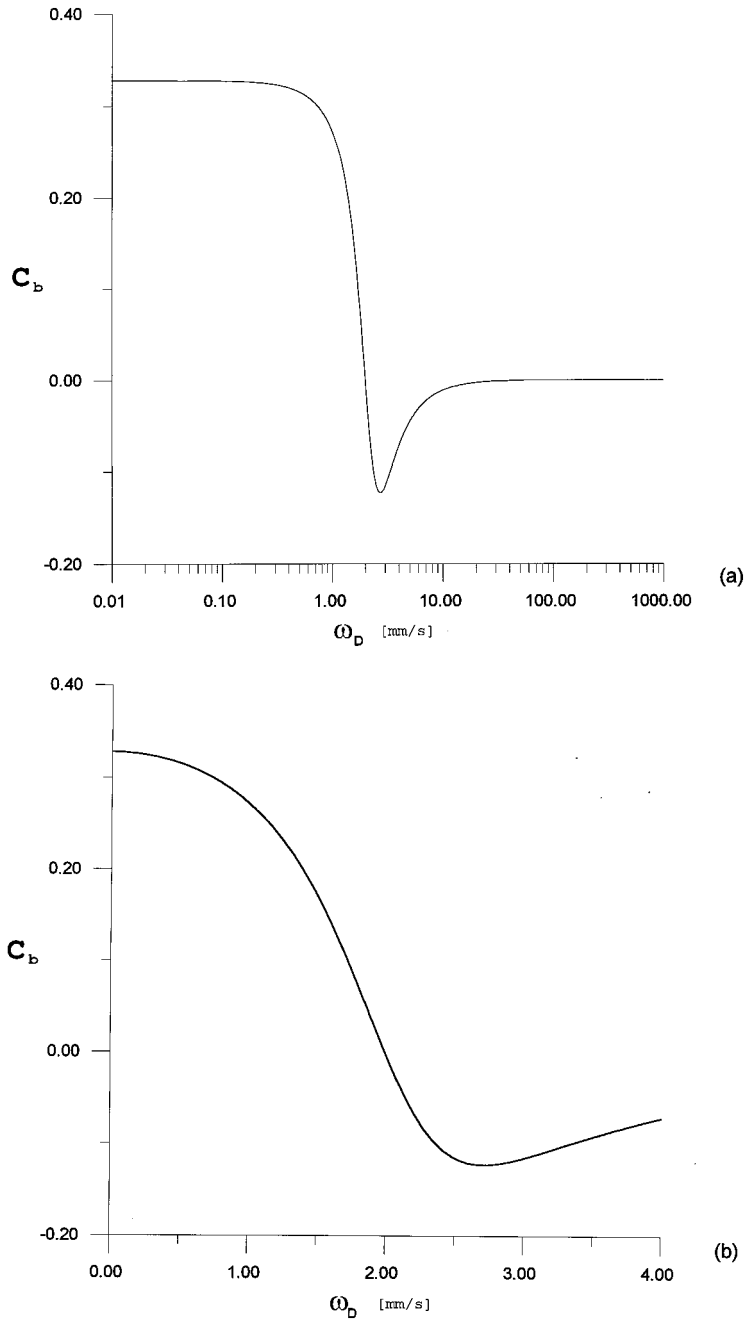

FIG. 7. C_b plotted versus ω_D for the same quadrupole coupling constants as those of Fig. 6: (a) broad range of ω_D, (b) narrow range of ω_D.

The last integral exists in the principal sense and the odd terms in the recoilless radiation density are due to the relaxation of the EFG.

The quantity $P(\overline{qv})$ is a directly measurable quantity versus v in a standard Mössbauer setup, i.e., it represents a detector count rate for a Doppler velocity v applied to either source or absorber in the direction defined by the wave vector $\overline{q}$. A variation of the q_0 due to the applied Doppler shift is negligible for typical velocity ranges. Positive velocities v correspond to the situation where the absorber is approaching the source, while negative velocities occur when the absorber is receding from the source.

Finally, one has to note that for the rutile structure the superoperator $\hat{\mathbf{R}}$ could be decomposed into $(-\{\omega_D[\gamma(\overline{q})+1/2]+iS\}\hat{1})$ and $\hat{\mathbf{R}}+\{\omega_D[\gamma(\overline{q})+1/2]+iS\}\hat{1}$, the latter having eigenvectors independent of $\overline{q}$ and eigenvalues $\lambda_\nu(\overline{q})+\{\omega_D[\gamma(\overline{q})+1/2]+iS\}$. Here, the symbol $\hat{1}$ denotes a unit operator of the proper dimension. Such a decomposition is possible due to the fact that the diffusion occurs within a single Bravais lattice.

For the 14.4 keV Mössbauer line in ^{57}Fe (being already equilibrated with the lattice) a ground-state nuclear level does not participate in the EFG relaxation ($I_e=3/2$, $I_g=1/2$, practically pure $M1$ transition, ξ almost equal zero) and hence, a relaxation is entirely due to the first excited nuclear level having doubly degenerated hyperfine sublevels (Kramers degeneracy). Thus, one obtains two ''doublets'' having the same line positions, albeit different linewidths (except for the ''static'' limit, where a single doublet is present). Figure 6 shows $\Gamma_1=(1/2)\{\Gamma-\Gamma_\nu(\overline{q}=G)\}$ for ν belonging to the ''narrow subset,'' $\Gamma_2=(1/2)\{\Gamma-\Gamma_\nu(\overline{q}=G)\}$ for ν belonging to the ''broad subset,'' and a ''doublet'' splitting Δ plotted

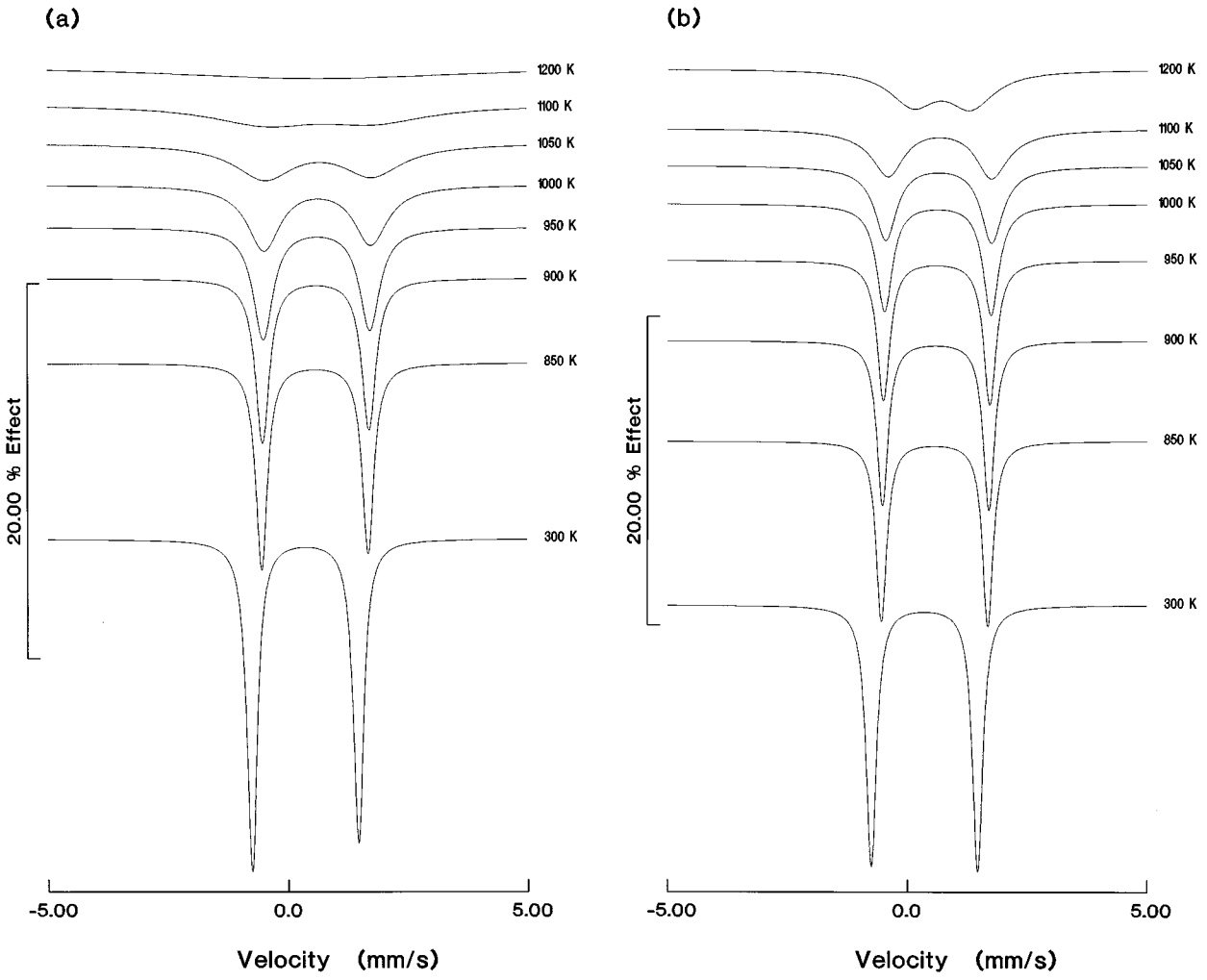

FIG. 8. Some spectra $P(\overline{qv})$ calculated for the 14.4 keV line in ^{57}Fe for a linear velocity scale v: (a) $R=0.01$, $\theta=22°$, $\phi=0°$, (b) $R=0.01$, $\theta=37$, $\phi=0°$, (c) $R=0.01$, $\theta=40°$, $\phi=0°$, (d) $R=100$, $\theta=40°$, $\phi=0°$, (e) $T=1100$ K, $\theta=40°$, $\phi=0°$.

versus frequency ω_D. All values have been rescaled by q_0^{-1} including adopted quadrupole coupling constants[13]

$$A_{zz}=\{(\mathbf{e}Q_e)/[4I_e(2I_e-1)]\}V_{zz}$$

and

$$A_{xx}=\{(\mathbf{e}Q_e)/[4I_e(2I_e-1)]\}V_{xx}$$

with $A_{zz}=-0.2379$ mm/s and $A_{xx}=-0.1281$ mm/s.

Figure 7 shows a relative contribution to the emission profile due to the broad component, i.e.,

$$C_b=\sum_{\substack{\text{broad}\\ \text{components}}}\langle b_\nu(\overline{q})\rangle_{\theta\phi}$$

(with $\langle\cdots\rangle_{\theta\phi}$ denoting averaging over all directions) calculated for a completely random ''powder'' sample and isotropic recoilless fraction and plotted versus ω_D rescaled by q_0^{-1}. One can clearly see that negative intensities occur in the emission profile. However, a total profile or a profile calculated for a particular polarization remains always nonnegative for all physically meaningful cases (at any frequency and in any direction in the case of a single crystal as well). One has to note that imaginary parts of the C_b amplitude and a corresponding C_n amplitude (narrow component) are always zero for the model considered here.

Such a behavior indicates that neither narrow nor broad components could be observed separately. A relaxation of the EFG driven by the diffusive motion mixes coherently hyperfine states belonging to the distinct sites. One could see as well that for the very fast relaxation C_b and Γ_1 tend to zero. This is a motional narrowing effect similar to the one observed by the nuclear magnetic resonance method.

Finally, Fig. 8 shows examples of spectra calculated for the following parameters[13] (all ''frequency'' parameters scaled by q_0^{-1}):

$$\Gamma_0=0.097 \text{ mm/s}, \quad t=2.0, \quad \Gamma=0.11 \text{ mm/s},$$

$$A_{zz}=-0.2379 \text{ mm/s}, \quad A_{xx}=-0.1281 \text{ mm/s},$$

$$a=4.594 \text{ Å}, \quad c=2.959 \text{ Å}, \quad q_0=7.30254 \text{ Å}^{-1},$$

$$\phi=0°$$

$$S=-0.3 \text{ mm/s at temperature } T=0 \text{ K},$$

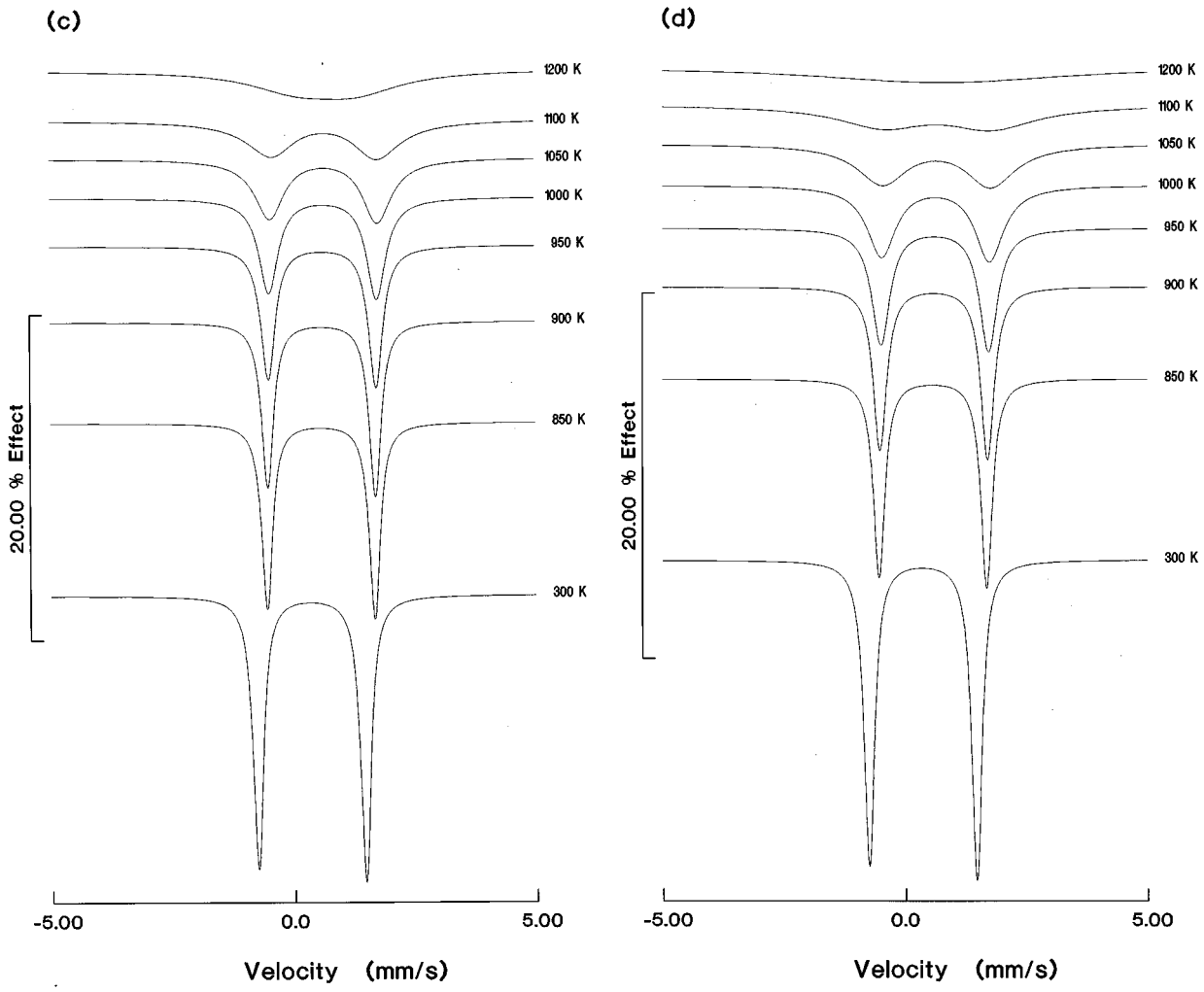

FIG. 8. (*Continued*)

$$B_{xx}=1.569\times10^{-3},\quad B_{yy}=2.044\times10^{-3},$$
$$B_{zz}=1.809\times10^{-3}\ \text{in}\ \text{Å}^2$$

(mean-squared displacements along xyz axes, respectively) at temperature $T=0$ K. A recoilless fraction $f_S(\overline{q})$ has been corrected for $\lambda=1.2$ for all spectra. Parameters B_{xx}, B_{yy}, B_{zz}, and S have been corrected for the temperature effect using a harmonic isotropic model with the parabolic density of phonon states (Debye model) having the effective cutoff (Debye) temperature $\theta_D=600$ K (adopted after Ref. 28). A shift S has been corrected solely for the second-order Doppler shift adopting the following mean-squared velocity:[29]

$$\langle v^2\rangle=5.576\times10^{10}\ (\text{mm/s})^2\quad \text{at}\ T=0\ \text{K}.$$

All corrections to linewidths due to the second-order Doppler shift at finite temperatures have been neglected as irrelevant in comparison to the intrinsic linewidths at meaningful temperatures.[30] A frequency ω_D has been taken as $\omega_D=\omega_D^0\exp[-(U/T)]$ with $\omega_D^0=1.871\times10^6$ mm/s and $U=16\,219$ K, i.e., for an oxygen saturated and thermodynamically stable TiO_2-rutile.[1] Quadrupole coupling constants are likely to remain weakly temperature dependent due to the oxidation state of substitutional iron (almost all of iron atoms) in the rutile structure with divalent anions. The parameter R strongly depends upon temperature, in principle. However, its value is likely to reach a saturation value at temperatures high enough for a diffusivity to be observable and hence, it appears to be almost temperature independent. Such a behavior has been observed by a tracer method for a diffusion of ^{59}Fe in oxygen-saturated rutile (TiO_2),[1] where the anisotropy of the diffusion coefficient was found to be very weakly dependent upon temperature (provided a sample was perfect enough to avoid blocking of channels). Results obtained by Sasaki, Peterson, and Hoshino[1] allow us to estimate R roughly as being close to 100 for the above-mentioned impurity-host system. The same results clearly show that the parameter R is temperature independent in the temperature range accessible experimentally. It has to be noted, that in the case of about 1–2 % effect a statistically relevant spectrum could be accumulated within about 24 h provided a source activity amounts to several mCi and a detector acceptance solid angle is of the order of several degrees. It is important to use thin samples in the direction of the emitted γ ray in order to minimize a self-absorption, the latter being due to the photoeffect mainly.

Figure 9 shows a spectrum distortion due to the typical experimental geometry. All corrections have been taken into account except detector geometrical effects and reemission

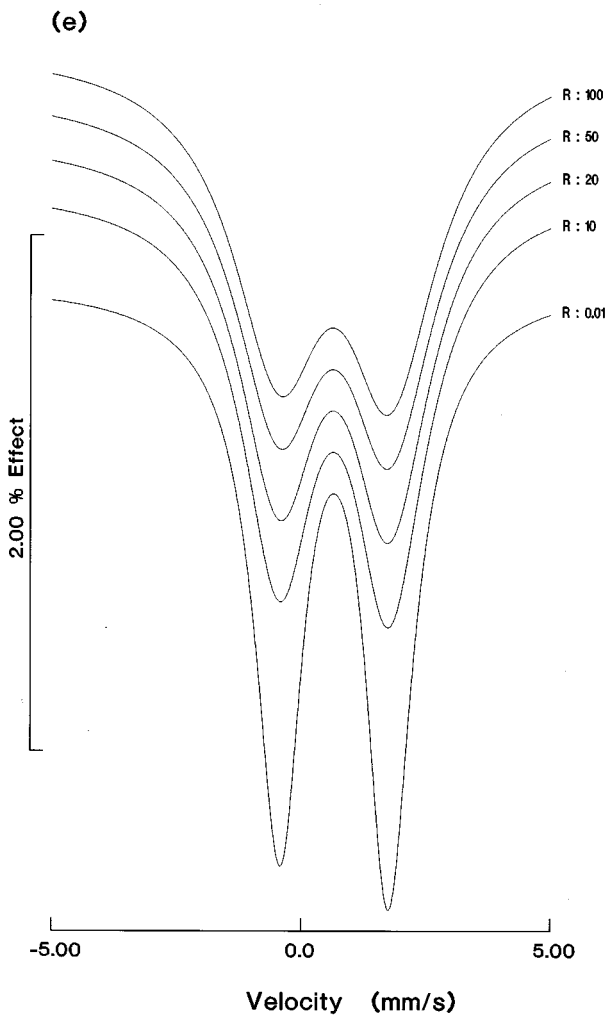

FIG. 8. (*Continued*).

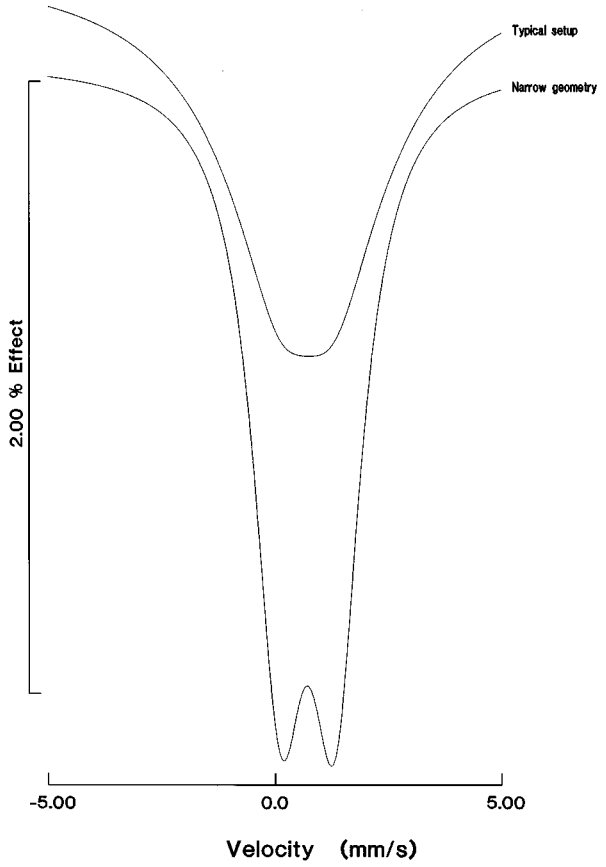

FIG. 9. Comparison of spectra calculated for $T=1200$ K, $\theta=35.6°$, and $R=100$ in the case of perfect (narrow) geometry and for a typical experimental setup; $\phi=0°$. Axes have the same meaning as in Fig. 8.

of the Mössbauer line (both elastic and inelastic components) from the absorber, and reaching the detector. The last effect would primarily affect $f_S(\overline{q})$ and t. One can conclude, that in the case of large R a special geometry might be necessary to obtain reliable results, i.e., one has to apply two-dimensional Soller collimators.[31] It should be noted that a direction chosen for the calculations of the geometrical effects is particularly sensitive to the changes in the polar and azimuthal angles. The smearing effect would be (fortunately) less pronounced in other directions. There are numerous parameters required to calculate geometrical effects and hence, we offer for those interested a special subroutine SCOLLIM which is able to calculate weights of the subspectra contributing to the final signal. Roughly speaking a typical setup consists of a rectangular source having dimensions 7×12 mm and a thickness 0.1 mm. A direction $\langle111\rangle$ is perpendicular to the source surface and the source is located 120 mm beneath a circular collimator having 15 mm diameter. The source is rotated around the axis parallel to the collimator plane in such a way, that a photon propagating along the collimator axis is emitted at the angle $\theta=35.6°$. The longer source dimension is almost parallel to the source rotation axis.

It is important to realize that the geometrical effects are largest in the directions where the function $\gamma(\overline{q})$ has deep minima restricted to the small area of the Ewald sphere. Such minima occur for long distances traveled by the impurity within a channel and hence, they appear for large values of the parameter R [see, Fig. 5(c)]. A significance of the geometrical smearing could be evaluated solely by performing suitable simulations. Hence, it is highly desirable to include geometrical effects in the procedure used to fit parameters of the model to the experimental data. A subroutine SCOLLIM conforms to such conditions provided an experimental geometry is well defined.

VIII. CONCLUSIONS

It has been found that a distribution of the impurity diffusing within an empty channel is governed by a simple exponential law depending solely upon the ratio of frequencies describing jumps within the channel and out of the channel, respectively. A reduced anisotropy of the diffusion coefficient depends solely upon the above ratio and the relationship between these two quantities is almost linear, see, Eq. (16). Hence, the above ratio could be found in the straightforward manner from the tracer data obtained for the single-crystal samples. For a very fast diffusivity in the channel the ratio of the above-mentioned frequencies becomes temperature independent. A frequency of the diffusive events is governed by the frequency of the impurity jumps into the

channel and hence, a reduced transversal diffusivity is governed solely by the above frequency.

A diagonal geometrical factor of the self-correlation function exhibits very narrow minima on the Ewald sphere for large values of the ratio R and a wave-vector transfer encompassing a significant number of the reciprocal points. Hence, a special experimental geometry might be necessary to obtain reliable results by the Mössbauer technique. These very narrow minima resemble an ''interference'' pattern originating from the large number of equally spaced scattering ''slits'' and the physics behind this phenomenon is actually very similar. A very fast semianalytical and phenomenological algorithm to calculate a self-correlation function has been developed.

It has been shown that the impurity diffusing on a single nonprimitive Bravais lattice might experience relaxation of the color. Such a color relaxation might lead to the reorientational relaxation of the EFG in the case of nonmagnetic materials. It is interesting to note that for the rutile structure the relaxational averaging of the EFG is incomplete even in the extremely fast relaxation limit. The rutile structure is the first known structure where the unique relationship between diffusivity and the color relaxation was found. The frequency of the latter is simply half of the diffusive event frequency. Hence, a diffusivity could be observed by the Mössbauer technique, even for the wave-vector transfer being one of the reciprocal-lattice vectors as the spectrum is perturbed by the EFG relaxation, the latter being driven solely by the diffusive events. A diffusion driven relaxation of the EFG mixes coherently hyperfine levels belonging to distant sites on the Bravais lattice. A motional narrowing effect appears for the EFG relaxation, while it is absent for a pure diffusive broadening due to the fact that the diffusive motion remains unbounded.

Due to the fact that the recoilless fraction is anisotropic the reorientational relaxation of the recoilless fraction occurs with the same frequency as the relaxation of the EFG. Hence, off-diagonal terms in the vibrational dynamics matrix appear. They are likely to be equal to the simple geometrical averages of the respective recoilless fractions as the time scale of the diffusive motion is much larger than the time scale of the vibrational motion. However, it is an example where the off-diagonal terms could be unambiguously defined. In order to observe the phase of the off-diagonal terms one has to look at the quantum (tunneling) diffusivity, the latter being seldom observable for such heavy impurities like Mössbauer atoms. For a classical limit relative phases are lost (averaged to zero) and one could see absolute values of the vibrational amplitudes solely.

ACKNOWLEDGMENTS

Dr. Bogdan Sepioł (Institut für Festkörperphysik der Universität Wien, Vienna, Austria) is warmly thanked for many helpful comments. This work has been financed by KBN (The National Committee for Scientific Research, Poland) under the Grant No. 2 P302 193 05.

*To whom all correspondence should be addressed. E-mail: sfrueben@cyf-kr.edu.pl ⟨Internet⟩.

[1] Jun Sasaki, N. L. Peterson, and K. Hoshino, J. Phys. Chem. Solids **46**, 1267 (1985).
[2] D. Wolf, Appl. Phys. Lett. **30**, 617 (1977).
[3] K. Ruebenbauer, B. Sepioł, and B. Miczko, Physica B **168**, 80 (1991).
[4] K. S. Singwi and A. Sjölander, Phys. Rev. **120**, 1093 (1960).
[5] C. T. Chudley and R. J. Elliott, Proc. Phys. Soc. London **77**, 353 (1961).
[6] J. W. Rowe, K. Sköld, H. E. Flotow, and J. J. Rush, J. Phys. Chem. Solids **32**, 41 (1971).
[7] R. Kutner and I. Sosnowska, J. Phys. Chem. Solids **38**, 741 (1977).
[8] R. Kutner and I. Sosnowska, Acta Phys. Pol. A **51**, 171 (1977).
[9] W. Nadler and K. Schulten, Phys. Rev. Lett. **51**, 1712 (1983).
[10] A. M. Afanas'ev and V. E. Sedov, Phys. Status Solidi B **131**, 299 (1985).
[11] B. Sepioł and G. Vogl, Phys. Rev. Lett. **71**, 731 (1993).
[12] M. Kwater, K. Ruebenbauer, and U. D. Wdowik, Physica B **190**, 199 (1993).
[13] M. Steiner, M. Köfferlein, W. Potzel, H. Karzel, W. Schiessl, G. M. Kalvius, D. W. Mitchell, N. Sahoo, H. H. Klaus, T. P. Das, R. S. Feigelson, and G. Schmidt, Hyperfine Interact. **93**, 1453 (1994).
[14] M. Blume, Phys. Rev. **174**, 351 (1968).
[15] H. Winkler and E. Gerdau, Z. Phys. **262**, 363 (1973).
[16] A. Gedikli, H. Winkler, and E. Gerdau, Z. Phys. **267**, 61 (1974).
[17] K. Ruebenbauer, Physica B **172**, 346 (1991).
[18] J. T. Day, J. G. Mullen, and R. C. Shukla, Phys. Rev. B **52**, 168 (1995).
[19] G. Albanese, F. Cavatorta, and A. Deriu, in *Proceedings XX Zakopane Winter School on Physics, Vol. 2*, edited by J. J. Bara, K. Ruebenbauer, and Z. Stachura (INP, Cracow, 1985), p. 255.
[20] R. A. Wagoner, B. Bullard, M. May, S. Dickson, and J. G. Mullen, Hyperfine Interact. **58**, 2687 (1990).
[21] A. M. Afanas'ev, V. D. Gorobchenko, and V. N. Peregudov, Hyperfine Interact. **5**, 469 (1978).
[22] M. Kwater, K. Ruebenbauer, and U. D. Wdowik, Physica B **190**, 209 (1993).
[23] S. Margulies and J. R. Ehrman, Nucl. Instrum. Methods **12**, 131 (1961).
[24] S. Margulies, P. D. Debrunner, and H. Frauenfelder, Nucl. Instrum. Methods **21**, 217 (1963).
[25] W. Henning, G. Baehre, and P. Kienle, Phys. Lett. B **31**, 203 (1970).
[26] J. L. Gimlett, H. E. Henrikson, N. K. Cheung, and F. Boehm, Phys. Rev. Lett. **42**, 354 (1979).
[27] J. G. Mullen, B. R. Bullard, and G. Schupp, in *Proceedings XXV Zakopane School on Physics, Vol. 1*, edited by J. Stanek and A. T. Pędziwiatr (World Scientific, Singapore, 1990), p. 18.
[28] C. J. Howard, T. M. Sabine, and F. Dickson, Acta Crystallogr. B **47**, 462 (1991).
[29] W. Potzel, in *Proceedings XX Zakopane Winter School on Physics, Vol. 2* (Ref. 19), p. 294.
[30] H. Wegener, in *Proceedings International Conference on MS, Vol. 1*, edited by D. Barb and D. Ţariňa (CIP, Bucharest, 1977), p. 203.
[31] J. G. Mullen (private communication).